Atomic structure and origin of chirality of DNA-stabilized silver clusters

Xi Chen *
Department of Applied Physics, Aalto University, Otakaari 1, 00076 Aalto, Finland

Mauro Boero
University of Strasbourg, Institut de Physique et Chimie des Matériaux de Strasbourg, CNRS, UMR 7504, 23 rue du Loess, F-67034 Strasbourg, France

Olga Lopez-Acevedo
Grupo de Física Computacional de Nanobiomateriales, Instituto de Física, Facultad de Ciencias Exactas y Naturales, Universidad de Antioquia UdeA; Calle 70 No. 52-21, 050010 Medellín, Colombia

(Received 23 February 2020; revised manuscript received 2 May 2020; accepted 8 May 2020; published 1 June 2020)

DNA-stabilized silver clusters (Ag:DNAs) have attracted much attention due to their unique sequence-dependent fluorescence and many potential applications; however, the understandings of their atomic structures and functional properties are still limited, which hamper the further development of the novel nanoclusters. Using the advanced computational methods, we propose three atomistic models for the Ag:DNAs, which all contain a four-electron silver core with a two-row planar shape stabilized by the nitrogen atoms in the DNA. By comparing experimental and time-dependent density functional theory-simulated circular dichroism spectra, we have confirmed that these core structures should commonly exist in the Ag:DNAs. We then analyze the electronic and optical properties of the clusters and discover that the silver to DNA transitions have essential contributions to the chiroptical properties of the clusters.

DOI: 10.1103/PhysRevMaterials.4.065601

I. INTRODUCTION

Protected noble-metal clusters play an increasingly important role in physics, chemistry, biology, and nanotechnology, since they have a wide spectrum of potential applications including, but not limited to, next-generation electronic devices, nanocatalysts, biochemical sensing, and innovative medical treatments [1]. Among the various protected noble-metal clusters, DNA-stabilized silver clusters (Ag:DNAs) stand out for their unique fluorescence properties. The Ag:DNAs only template clusters of ∼10 Ag atoms by 10–20 nucleotides [2–6]; however, these fluorescent conjugates have been tailored to emit light from the blue to near-infrared range by tuning DNA sequence and length [2–4,7]. Some clusters also have high fluorescence quantum yields and good photostability. These properties, combined with low toxicity, low synthesis costs, small cluster sizes, and natural compatibility with DNA, enable many exciting applications and cope with the worldwide request for sustainable technology with low environmental impact [2,3].

They are particularly promising candidates for fluorescent sensors of gene mutations [8,9], metal ions [10], and biomolecules [11]. They are also emerging in applications as logic devices [12] and cell labeling [13]. Despite the field's rapid growth, the limited knowledge of the cluster structure is a stumbling block to further development of the Ag:DNAs. An atomic-level understanding of the structure and functional properties will be instrumental in guiding the realization of these novel hybrid nanomaterials.

Structural arrangements of Ag:DNAs are particularly difficult to obtain experimentally via crystallization and only very recently have the first crystal structures been reported [14,15]. Therefore, theoretical calculations using quantum chemistry methods appear most promising to propose geometries and interpret the experimental results. In this context, circular dichroism (CD) spectroscopy accompanied by computational modeling is a proven, powerful tool for characterizing the structures of DNA-related materials. For example, by comparing computed with measured CD, we have inferred the atomic structures of Ag^{+}-mediated cytosine and guanine duplexes [16,17]. In 2014, Gwinn's group reported the structurally sensitive, chiroptical activity of four Ag:DNAs [18]. Although the DNA templates vary in both length and sequence, the clusters share ubiquitous features in CD spectra, including a positive peak overlying the lowest optical absorption peak around 2.0 eV and a negative peak between 3.0 eV and 3.5 eV. This result indicates that there are common structural features in the Ag:DNAs and provides us extreme valuable experimental data for comparison (Fig. 1).

In this work, we aim to understand the origin of the common structural features of the fluorescent Ag:DNAs by simulating the atomic structure and CD of the clusters. The construction of the models used in our simulations was

*xi.6.chen@aalto.fi

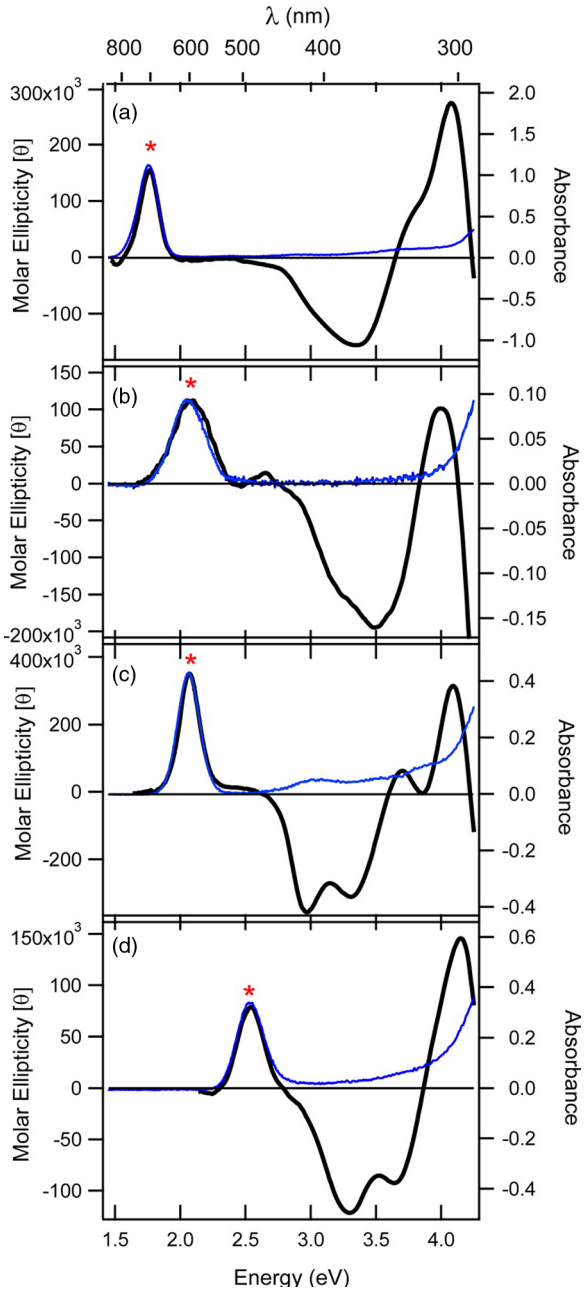

FIG. 1. CD (black) and absorption (blue) spectra of pure cluster solutions S1 (a), S2 (b), S3 (c) (aqueous solution), and S4 [(d); 50 MeOH]. A positive CD peak overlies the collective longitudinal cluster absorbance peak (red stars). S1: CCCACCCACCCGCCCA, 12 Ag^0, 8 or 9 Ag^+; S2: GGCAGGTTGGGGTGACTAAAAACCCTTAATCCCC, 6 Ag^0, 9 Ag^+; S3: CACCGCTTTTGCCTTTTGGGGACGGATA, 6 or 7 Ag^0, 8 or 9 Ag^+; S4: TGCCTTTTGGGGACGGATA, 4 Ag^0, 6 Ag^+. The figure is taken from [18] with permission.

guided by the following previous experiments. (1) Cytosine- or guanine-rich DNA templates relate to form bright clusters [19,20]. Machine learning from the large experimental databases has found that there are discriminative motifs for bright clusters [19]. These motifs contain three to five bases, for example: CCC, CCCC, CCG, GCG, GGCAC *et al.* (2) The relation between the charge and number of silver atoms from mass spectrometry suggests that the clusters contain both neutral and cationic silver atoms [21]. (3) The green and red fluorescent clusters have enhanced abundances with neutral Ag numbers $N_0 = 4$ and $N_0 = 6$ [7]. (4) Multiple experimental results evidence that the clusters have most probably a rod shape [7,21].

Starting from the experimental information, we did a thorough investigation of the electronic properties of several candidate structures. Our analysis evidenced three complexes which can be suitable geometries for an atomic scale description of Ag:DNAs. Their atomic structures, optical absorption and circular spectra, and electronic structures will provide a solid ground to assess the reliability of these structures and the discussion of the outcome of these simulations will be given in the following sections.

II. COMPUTATIONAL METHODS

Since there is an enormous amount of base-pair combinations that DNA allows, constructing and simulating all the possible model sequences is a nearly impossible task. To simplify the problem, we considered all experimental results listed in the Introduction and built our initial models for simulation. We chose the cytosine duplex C_6-C_6 six cytosine nucleobases per DNA strand, $-10e$, as our DNA template, because of the known experimental fact (1). Specifically, cytosine-rich DNA templates have been reported to form bright clusters and CCC, CCCC are discriminative motifs in DNA for bright clusters. The number of possible conformations of the Ag atoms increase exponentially with the amount of Ag atoms; thus we limited our study to systems having 6–8 Ag atoms. Due to the experimental evidences (2) and (3), we set four neutral Ag atoms in the model systems, and other Ag atoms were considered as Ag cations. The three systems have a total number of silver atoms of 6, 7, and 8, and a value of net charges of $-8e$, $-7e$, and $-6e$, respectively. Because of the charge assignment, we expect our systems will form four-electron Ag clusters, which will be confirmed later by Bader charge analysis. The discrimination between Ag atoms and Ag cations here is only used to define the total charge of the system. In our simulations, we imposed the net charge of the system, and the charge of each atom is a consequence of the DFT methodological formulation.

The initial structures were built based on our previous studies of cytosine-Ag^+ duplex [17,22] with the help of 3DNA software [23]; then density functional theory (DFT) optimization and quantum mechanics/molecular mechanics (QM/MM) molecular dynamics were performed as implemented in the CP2K package [24] to obtain their atomic structures.

Sixteen different initial configurations were considered and 6.5 ps QM/MM dynamical simulations were performed to assess the stability of the most promising ones. To exclude the equilibration phase, only the last 2.0 ps of the obtained trajectories were used for the postprocessing analysis. In the reported experimental spectra, the Ag:DNAs share ubiquitous features independent of the DNA templates and the number of Ag atoms, including a positive peak overlying the lowest optical absorption peak around 2.0 eV, followed by a negative peak between 3.0 eV and 3.5 eV (Fig. 1). These similar spectra

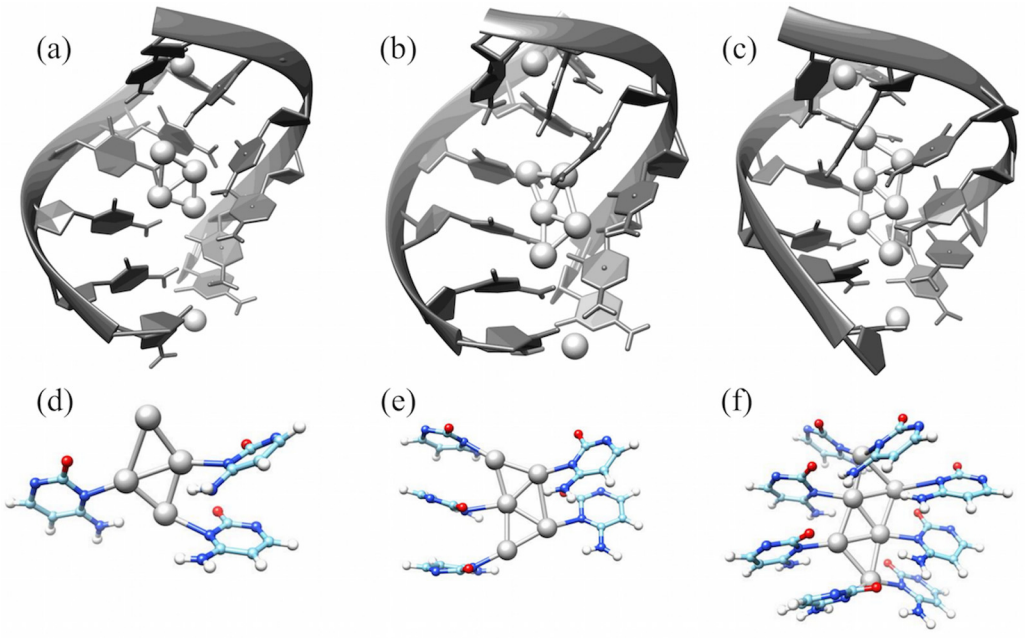

FIG. 2. (a)–(c) Structure of the Ag_4^0@C_6-[Ag^+]$_2$-C_6, Ag_5^{+1}@C_6-[Ag^+]$_2$-C_6, and Ag_6^{+2}@C_6-[Ag^+]$_2$-C_6; (d)–(f) the Ag core and their neighbor atoms in the Ag:DNAs, respectively.

evidence that there are some common Ag structures in the Ag:DNAs. Our search for suitable structures continued until we found those specific clusters able to closely reproduce the experimental CD and optical spectra.

All QM/MM simulations were done with the CP2K code [24]. The DNA and Ag atoms were considered as the quantum subsystem and treated at the Kohn-Sham DFT level. Na^+ were used as counterions and the number of them was chosen to set the charge of the whole system to be neutral. The solvent H_2O molecules and the Na^+ counterions were considered as the classical surrounding system and their interactions described by a standard AMBER classical force field [25]. Valence electronic orbitals and densities were expanded on a mixed Gaussian and plane-wave basis set [26,27]. In particular, for the localized part, we adopted a double-ζ valence plus polarization (DZVP) basis sets of the MOLOPT type [28]. Norm-conserving Goedecker-Teter-Hutter (GTH) pseudopotentials were used to describe the core-valence interaction [29–31], and the Perdew-Burke-Ernzerhof (PBE) functional [32] was used to express the exchange and correlation interactions, complemented by the Grimme's D3 correction [33] to account for the long-range van der Waals dispersions. The electron density was expanded in an auxiliary set of plane waves with a cutoff energy of 300 Ry. The electrostatic interactions between the QM and MM subsystems were modeled by charge sets of the Amber force field employing the electrostatic coupling procedure implemented in the QM/MM module in CP2K to account for periodic boundary conditions correctly [34,35]. The QM boxes were about $36.0 \times 36.0 \times 40.0$ Å^3, while the MM boxes were about $46.0 \times 46.0 \times 46.0$ Å^3 filled with water molecules. The dispersion interactions between the DNA-silver system and MM atoms were reproduced by an empirical potential of the Lennard-Jones type using AMBER parameters.

Molecular dynamics (MD) simulations were performed within the canonical (NVT) ensemble at 300 K using a step of 0.5 fs. Before the QM/MM simulations, we had preequilibrated the solvent structures for 2.0 ns at the MM level, keeping the DNA-Ag systems in their DFT-optimized vacuum structures. Then the QM/MM simulations were performed for 6.5 ps. The last 2.0 ps of trajectories were used for analysis. We performed molecular dynamic simulation, as opposed to static optimizations, because Ag:DNAs are mainly existing in solution, and we need to cope with the intrinsic dynamical nature of these solvated structures.

The electronic properties, optical absorption spectra and ECD were calculated using a DFT code GPAW [36] which is based on the projected augmented wave method. The wave functions were described with real-space uniform grids. The grid spacing was 0.2 Å in this work. The silver and DNA-base atoms were included in all the simulations, where H atoms replaced the sugar-phosphate backbones. Per atoms, the electronic configurations of valence electrons are H($1s^1$), O($2s^2 2p^4$), C($2s^2 2p^2$), N($2s^2 2p^3$), and Ag($4p^6 4d^{10} 5s^1$). The optical absorption spectra and ECD were calculated using the linear-response time-dependent DFT implemented in GPAW [37] with the GLLB [38] and LB94 [39] exchange-correlation functional.

III. RESULTS AND DISCUSSIONS

Figures 2(a)–2(c) show the structures of three Ag:DNAs: Ag_4^0@C_6-[Ag^+]$_2$-C_6, Ag_5^{+1}@C_6-[Ag^+]$_2$-C_6, and Ag_6^{+2}@C_6-[Ag^+]$_2$-C_6 after 6.5 ps QM/MM simulations. In all the Ag:DNAs, the central Ag atoms form a two-row planar core located in the center of the DNA double strands. The top and bottom Ag atoms, instead, turn out to be located in between

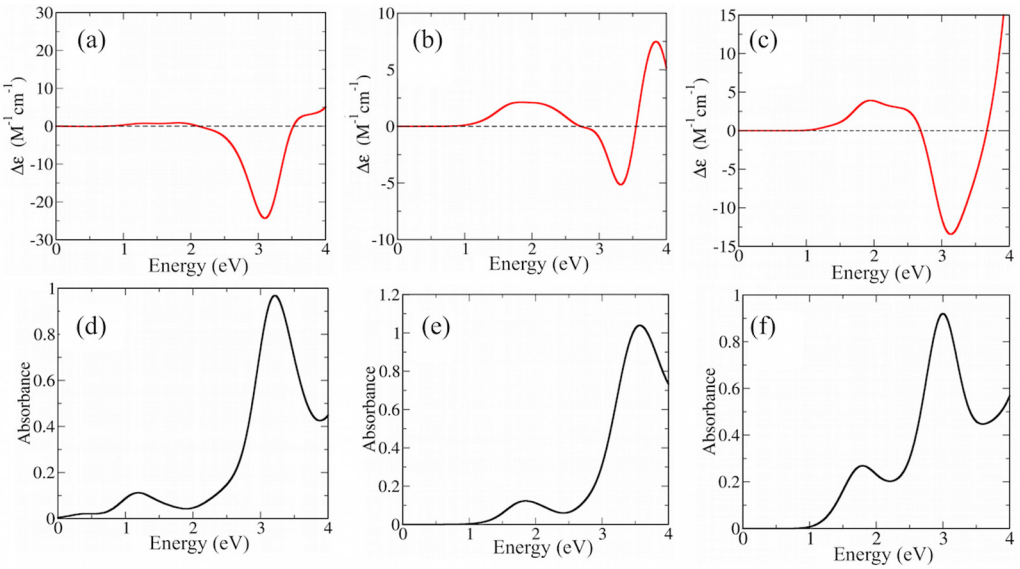

FIG. 3. (a)–(c) Calculated CD and (d)–(f) the calculated optical absorption spectra of the Ag_4^0@C_6-[Ag^+]$_2$-C_6, Ag_5^{+1}@C_6-[Ag^+]$_2$-C_6, and Ag_6^{+2}@C_6-[Ag^+]$_2$-C_6.

the cytosine pairs, thus acting as a sort of glue atoms bridging together the two DNA strands.

In the Ag_5^{+1}@C_6-[Ag^+]$_2$-C_6 and Ag_6^{+2}@C_6-[Ag^+]$_2$-C_6 all the central Ag atoms bind to N atoms as shown in Figs. 2(e) and 2(f), while in the Ag_4^0@C_6-[Ag^+]$_2$-C_6, three out of four central Ag atoms bind to N atoms as shown in Fig. 2(d). The average Ag-Ag distances are 2.78 ± 0.09 Å in the Ag_4^0@C_6-[Ag^+]$_2$-C_6, 2.79 ± 0.14 Å in the Ag_5^{+1}@C_6-[Ag^+]$_2$-C_6, and 2.80 ± 0.08 Å in the Ag_6^{+2}@C_6-[Ag^+]$_2$-C_6 and the average Ag-N bond lengths are 2.36 ± 0.03 Å, 2.34 ± 0.05 Å, and 2.40 ± 0.09 Å in the clusters, respectively. Similar Ag-Ag and Ag-N distances were observed in the crystal structures of Ag:DNAs [14,15]. We have found no evidence of O-Ag bond in the systems all along with our simulations. This is an indication that N atoms present in the DNA structure play a central role in stabilizing the Ag atoms in the Ag:DNAs. This finding agrees with the reported DNA-Ag structure [15] and our simulations in cytosine-Ag^+ and guanine-Ag^+ duplex [16,17].

In all the initial geometries considered in the present work, each DNA base pair was bound to at most one single Ag. The structures in Fig. 1 are, instead, the result of the QM/MM dynamics. The Ag_4 and Ag_5 core in our Ag:DNAs clusters have the same diamond and trapezoidal shapes as the bare Ag_4 and Ag_5 clusters predicted by former *ab initio* calculations [40]. At variance with these clusters, the difference was found for Ag_6 with respect to the isolated Ag_6. This discrepancy is due to the fact that the surrounding DNA duplexes impose a constraint to the possible Ag_6 conformations, orienting it toward a rodlike shape. Another remarkable feature is the trapezoidal Ag_5 core we found in our computational investigation. In fact, this specific shape was indeed observed in the first reported Ag:DNAs crystal cluster [15]. These previous studies provide strong support and a solid benchmark to our QM/MM studies and can be regarded as an assessment of the reliability of our computational setup. Yet, we have to stress the fact that the intrinsic complexity and flexibility of DNA allow for even the same DNA strand to accommodate different quantities and arrangements of Ag atoms [4]. Thus we cannot pretend to be exhaustive, and other types of Ag clusters cannot be ruled out.

The optical absorption and CD spectra were calculated using the linear-response time-dependent density functional theory (TDDFT) with adiabatic Gritsenko–van Leeuwen–van Lenthe–Baerends–solid-correlation (GLLBSC) exchange-correlation functional [38,41]. The functional was recommended for noble metal clusters because it introduces an orbital-energy dependent localization of the exchange hole and describes *d*-orbital more accurately. Former studies were able to show that the GLLBSC functional provides more accurate predictions of the optical absorption spectra of Ag clusters with respect to both the local density approximation (LDA) and the generalized gradient approximations (GGA) [42]. On this ground, we made our choice for the present work. Additional details are given in the Computational Methods section.

Figure 3 shows the calculated average spectra of the clusters from the five snapshots in the last 2.0 ps QM/MM simulations (4.5 ps, 5.0 ps, 5.5 ps, 6.0 ps, and 6.5 ps). The CD of the individual snapshots can be found in Fig. S1. The CD of the Ag_4^0@C_6-[Ag^+]$_2$-C_6 has a pronounced negative peak around 3.0 eV and a much smaller positive peak around 1.5 eV [Fig. 3(a)]. The Ag_5^{+1}@C_6-[Ag^+]$_2$-C_6 and the Ag_6^{+2}@C_6-[Ag^+]$_2$-C_6 both have the reported ubiquitous chiroptical features of the Ag:DNAs [18]: the first positive peak in the CD is around 2.0 eV overlying with the first peak in the optical absorption spectrum, and the second negative peak is around 3.0 eV [Figs. 3(b), 3(c) and Figs. 3(e), 3(f)]. This striking similarity indicates that this type of Ag_5 and Ag_6 core could commonly exist in the Ag:DNAs.

To verify whether the selected five snapshots were enough to reach an acceptable convergence of the average CD's main features, we sampled other additional two sets of uncorrelated snapshots of Ag_6^{+2}@C_6-[Ag^+]$_2$-C_6 and repeated the calculations for comparison. More precisely, these snapshots were sampled from the QM/MM trajectory, starting from

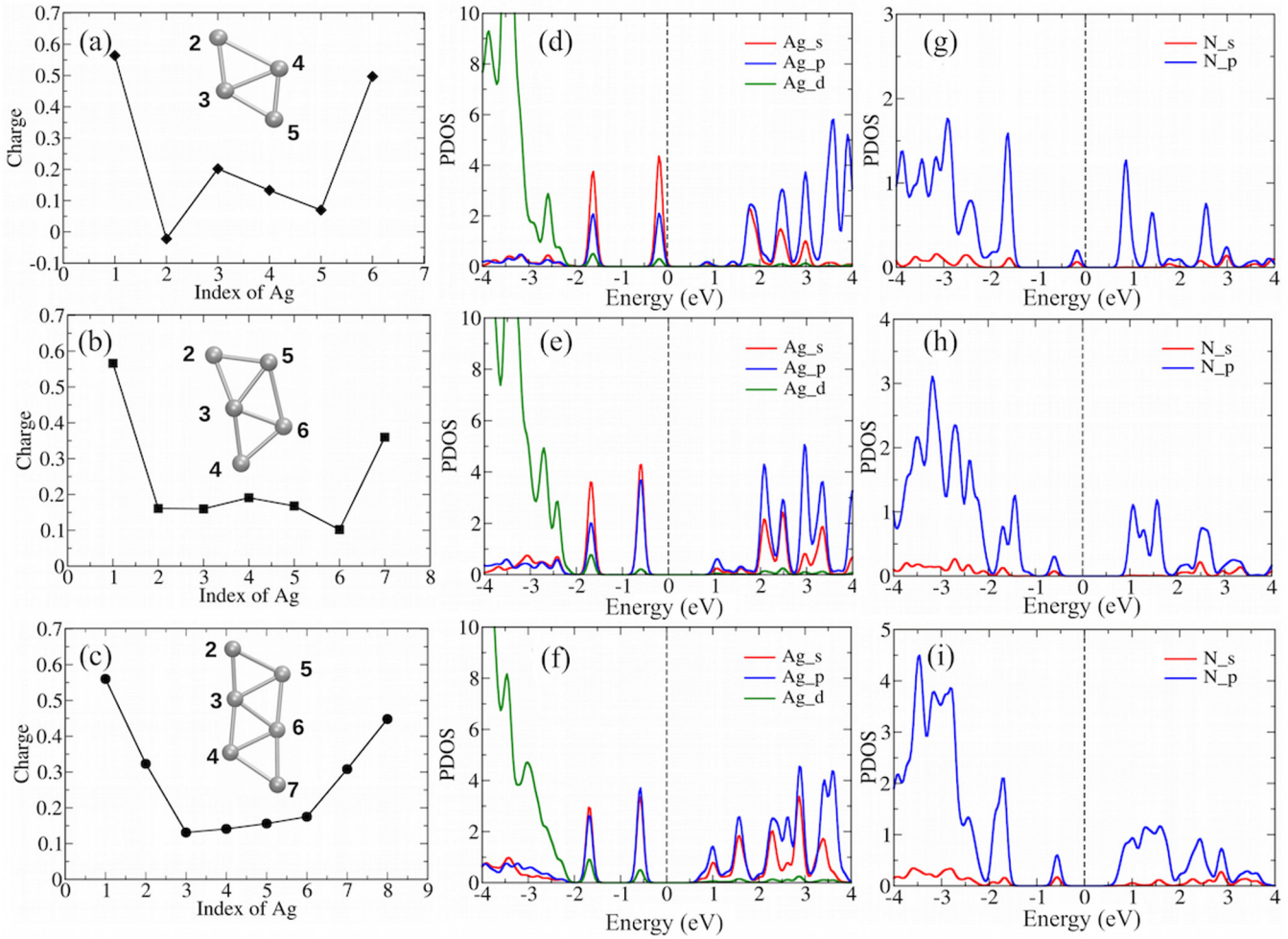

FIG. 4. (a)–(c) Bader charges of the Ag atoms in the Ag_4^0@C_6-[Ag^+]$_2$-C_6, Ag_5^{+1}@C_6-[Ag^+]$_2$-C_6, and Ag_6^{+2}@C_6-[Ag^+]$_2$-C_6. The top Ag atom was marked by **1** and the bottom Ag was marked by **6**, **7**, and **8**, respectively. The labeling of the Ag core atoms can be seen in the inset of the figures. (d)–(f) The PDOS of the core Ag atoms and (g)–(i) the PDOS of their neighbor N atoms in the Ag_4^0@C_6-[Ag^+]$_2$-C_6, Ag_5^{+1}@C_6-[Ag^+]$_2$-C_6, and Ag_6^{+2}@C_6-[Ag^+]$_2$-C_6.

4.2 ps and 4.3 ps, respectively, and collected at regular time intervals of 0.5 ps. The result of this comparative analysis is summarized in Fig. S2(a) [43], where it is evident that the three average CD spectra are qualitatively identical. In order to check if and to what extent the chiroptical features of the clusters depend on the exchange-correlation functional, we repeated the calculations of both the optical spectra and the CD of Ag_6^{+2}@C_6-[Ag^+]$_2$-C_6 with a GGA-type functional LB94 [39]. The result of these auxiliary calculations is a shift of the peaks in the spectra to the lower energies [Figs. S2(b) and S2(c) [43]]. This can be ascribed to the formulation of the LB94 functional, which tends to underestimate the Kohn-Sham band gap. Nonetheless, the main features are preserved, with a positive peak followed by a negative one in the CD [see Fig. S2(b) [43]].

The three clusters share the same type of atomic structure. To understand whether or not these similar structural properties correspond to similar electronic properties, we calculated the Bader charges and the projected density of states (PDOS) of the atoms in the clusters. The Bader charges of the Ag atoms are shown in Figs. 4(a)–4(c), in which the different numbers mark the central core Ag atoms in the clusters. A feature that can be easily remarked is that the top and bottom Ag atoms have larger positive values of the local charge than the Ag atoms located in the center of the DNA double strands. Specifically, in our case, the top and bottom Ag atoms are clearly cations in the three Ag:DNAs. In the Ag_4^0@C_6-[Ag^+]$_2$-C_6, the Ag3, Ag4, and Ag5 have small positive charges, while the Ag2 which is not closely bound to N atoms is in a neutral state and, as such, is really an Ag atom and not a cation. In the Ag_5^{+1}@C_6-[Ag^+]$_2$-C_6, all the Ag atoms located in the center of the cluster are slightly positive (charge $<0.2e$). In the Ag_6^{+2}@C_6-[Ag^+]$_2$-C_6, the Ag3, Ag4, Ag5, and Ag6 have small positive charges making them closer to a neutral Ag atom than to a cation, while Ag2 and Ag7 are characterized by intermediate charge states and, as such, partially ionized. In order to check the reliability of the charges obtained by a GGA-type of functional, we extracted one snapshot of Ag_6^{+2}@C_6-[Ag^+]$_2$-C_6 and recalculated the electronic structure and the Bader charges of the atoms at the hybrid PBE0 functional level, using the auxiliary density matrix methods (ADMM) implemented in CP2K [44]. PBE0

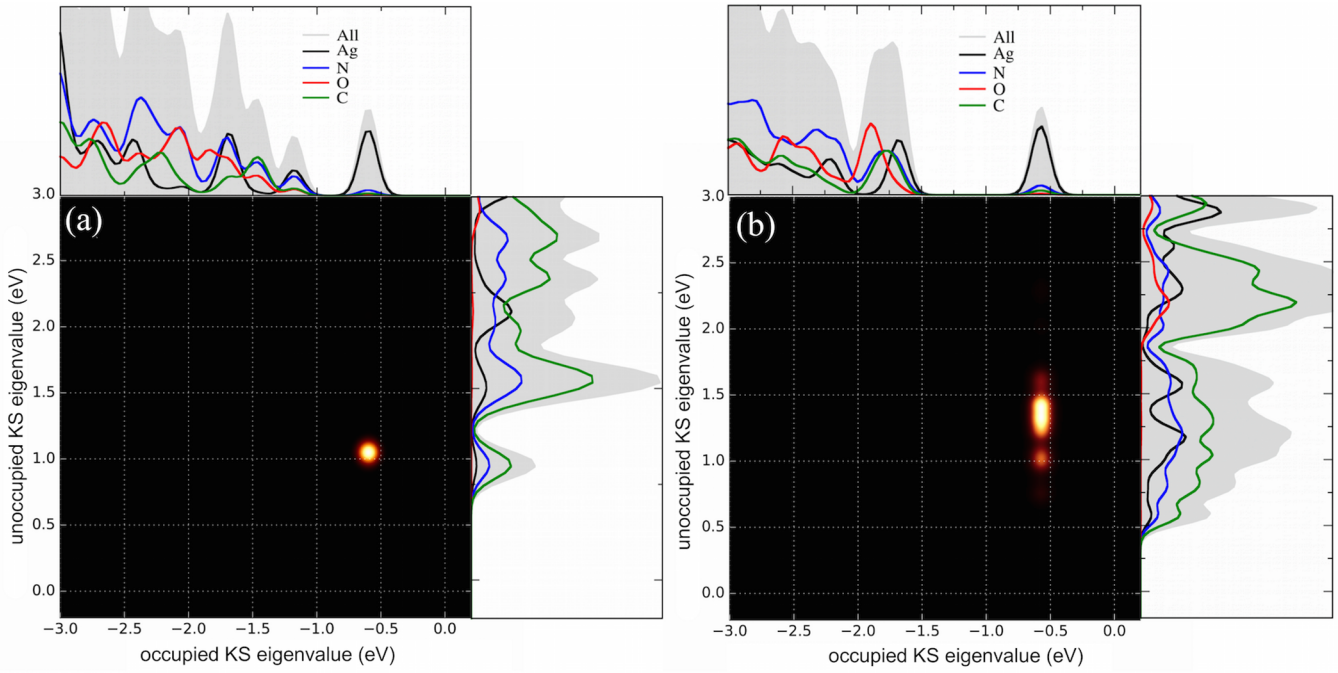

FIG. 5. (a) Transition contribution map of the $Ag_5^{+1}@C_6$-$[Ag^+]_2$-C_6 at 1.7 eV and (b) the transition contribution map of the $Ag_6^{+2}@C_6$-$[Ag^+]_2$-C_6 at 2.0 eV. The horizontal PDOS are for the occupied states, while the vertical PDOS are for the unoccupied states in the Ag:DNAs.

results turn out very similar to those obtained via LB94. The values of charges provided by PBE0 are plotted in Fig. S4 [43]. If we consider the top and bottom silver atoms as cations and the central Ag atoms sharing the rest charges, the central Ag cores can be written as Ag_4^0, Ag_5^{+1}, and Ag_6^{+2}. They are all four-electron systems.

This rich variety of charge states characterizing the Ag atoms framed in double-strand nucleic acids escapes any classical simulation reported so far, in which a unique parametrization of the Ag charge is assumed for any Ag atom in whatever position. This raises at least a warning about the validity of the use of these classical force fields for wired DNA and discloses new scenarios in the arrangement and electrostatics that Ag atoms can experience when framed inside double-strand nucleic acids.

The PDOS of the central Ag atoms and their neighbor N atoms are given in Figs. 4(d)–4(i), in which the 0.0 eV is set to be the Fermi level. The structures were picked from the snapshot at 6.0 ps in the QM/MM trajectories. As the size of the Ag core increases, the calculated highest occupied molecular orbital (HOMO)–lowest unoccupied (LUMO) band gaps increase from 0.4 eV in the $Ag_4^0@C_6$-$[Ag^+]_2$-C_6 to 1.2 eV in the $Ag_5^{+1}@C_6$-$[Ag^+]_2$-C_6 and $Ag_6^{+2}@C_6$-$[Ag^+]_2$-C_6. The PDOS of the Ag atoms in all the clusters has one peak originating from the contributions of s, p orbitals in HOMO states, and another peak between −1.0 eV and −2.0 eV [Figs. 4(d)–4(f)]. The Ag atoms represent the major contribution to the HOMO state, whereas the N atoms contribute more to the unoccupied states located just above the Fermi level [Figs. 3(g)–3(i)]. The features of PDOS suggest that the low-energy electronic transitions may occur from the Ag atoms to the DNA.

In order to get insight into the optical properties of the clusters, we analyzed the transitions corresponding to the first peak in the optical spectra (where also lies the first CD peak) of the $Ag_5^{+1}@C_6$-$[Ag^+]_2$-C_6 and $Ag_6^{+2}@C_6$-$[Ag^+]_2$-C_6. Figure 5(a) shows the transition contribution map of the $Ag_5^{+1}@C_6$-$[Ag^+]_2$-C_6 at 1.7 eV and Fig. 5(b) shows the transition map of the $Ag_6^{+2}@C_6$-$[Ag^+]_2$-C_6 at 2.0 eV. The structures were taken from the snapshot at the 6.0 ps in the QM/MM trajectory, and the corresponding spectra can be found in Fig. S3 [43]. From the transition maps, we can identify the origin of the first peaks featured in the optical absorption spectra and the CD of the Ag:DNAs. These peaks arise from the transitions between the HOMO Ag states and the unoccupied states whose major contribution comes from the atoms belonging to the DNA moiety. This is a clear indication that silver-to-DNA transitions occur and they contribute to the chiroptical properties of DNA-Ag clusters below 3.0 eV, which is in contrast to the current opinion, so far based on assumptions, about the fact that low-energy transitions are due exclusively to Ag atoms.

To confirm our findings and further check our conclusion, we computed the CD and optical absorption spectra of the bare Ag_4^0, Ag_5^{+1}, and Ag_6^{+2} clusters. The atomic structures were extracted from the same snapshots as in Fig. 3 in which all atoms apart from the Ag were removed. From Fig. 6, it is evident that both the optical absorption spectra and the CD are remarkably different from those of the Ag:DNAs. The first absorption peak in $Ag_4^0@C_6$-$[Ag^+]_2$-C_6 and $Ag_6^{+2}@C_6$-$[Ag^+]_2$-C_6 between 1.0 eV and 2.0 eV is missing in Ag_4^0 and Ag_6^{+2}. The first two peaks in CD of $Ag_5^{+1}@C_6$-$[Ag^+]_2$-C_6 and Ag_5^{+1} have opposite signs. This corroborates and confirms what we inferred. Namely, the DNA-Ag interactions play the prominent role in tuning the chiroptical properties of the Ag:DNAs' systems. We can also observe that the DNA bases arrange chirally around the Ag atoms and this chirality

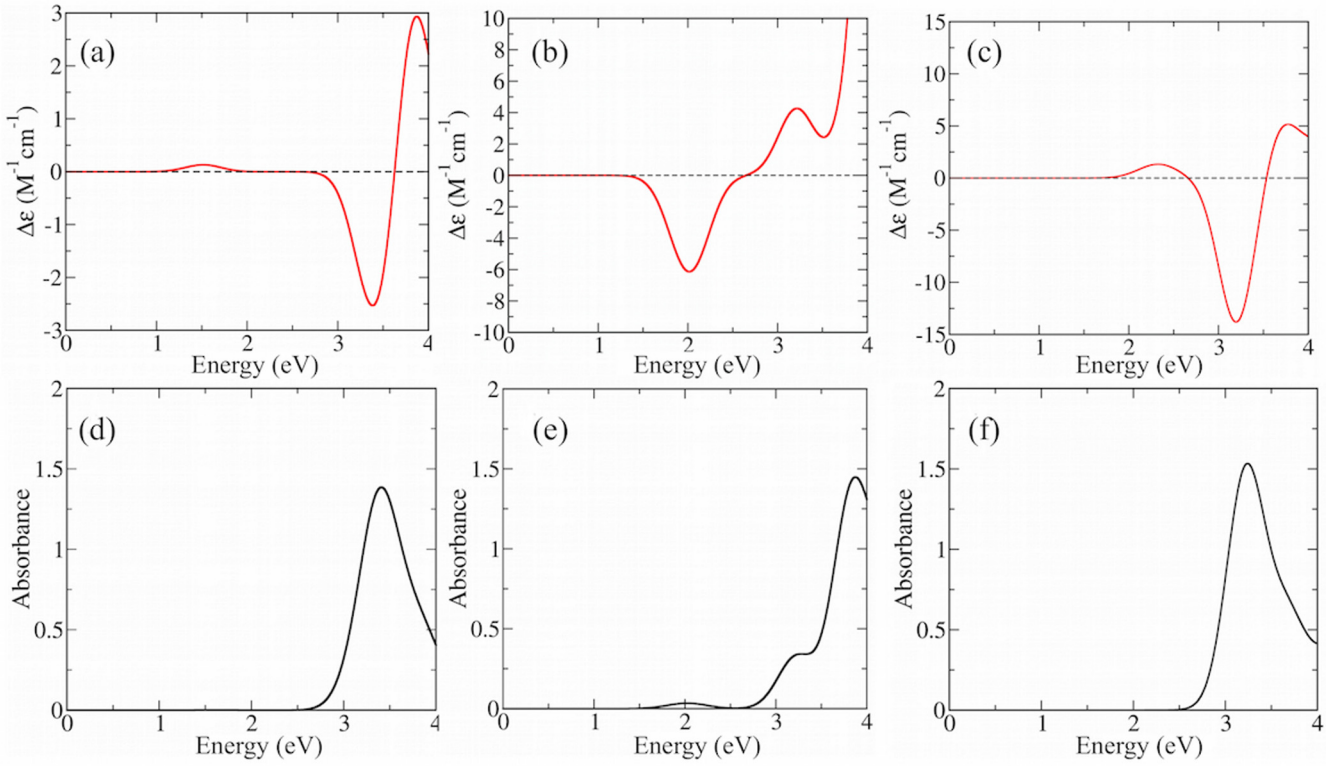

FIG. 6. (a)–(c) Calculated average CD of Ag_4, Ag_5^{+1}, and Ag_6^{+2}; (d)–(e) the calculated average optical spectra of Ag_4, Ag_5^{+1}, and Ag_6^{+2}.

is likely to be at the origin of the ECD observed in the clusters, with N atoms being plausible chiral centers in the Ag:DNAs.

IV. SUMMARY

In summary, using the best computational tools available, we have discovered three attractive Ag:DNAs. They all have an Ag core with a two-row planar shape. The clusters which have the Ag_5^+ or Ag_6^{+2} core give the optical absorption and ECD spectra representing the ubiquitous chiroptical features of Ag:DNAs observed in the experiments, indicating these core structures should be common in the Ag:DNAs. However, DNA is very flexible and has enormous sequence space; we expect other interesting atomic models of Ag:DNAs to be discovered in the future.

Besides the similar structures, we found the clusters also share similar electronic properties. In all the clusters, the Ag atoms represent the major contribution to the HOMO state, while the DNA atoms contribute more to the unoccupied states located just above the Fermi level. The features of PDOS suggest that the low-energy electronic transitions are from the Ag atoms to the DNA. The Ag atoms in the clusters have a rich variety of charge states. They can be close to neutral Ag atoms or Ag cations, or partially charged. If we consider the top and bottom silver atoms as cations, the central Ag cores are all four-electron systems.

We have calculated the transition map and analyzed the original of the chirality of the clusters. The Ag-to-DNA transitions have essential contributions to the low-energy transitions in the optical spectra and CD.

This work provides an atomic-level understanding of Ag:DNAs, which is an important step towards the rational design of Ag:DNAs. Our study also shows that the combined QM/MM and TDDFT computational methods can serve as virtual experiments to discover the new structure and understand the properties of Ag:DNAs.

ACKNOWLEDGMENTS

This work was supported by the Academy of Finland Projects Grants No. 308647 and No. 314298. We thank CSC, the Finnish IT Center for Science Espoo, for computational resources. M.B. thanks the HPC Mesocentera at the University of Strasbourg funded by the Equipex Equip@Meso project (Programme Investissements d'Avenir) and the CPER Alsacalcul/Big Data, and the Grand Equipement National de Calcul Intensif (GENCI) under allocation Grant No. DARI-A6 A0060906092. X.C. and O.L.-A. thank Prof. E. G. Gwinn, Dr. Stacy. M. Copp, and Dr. S. M. Swasey for the inspiring discussions. X.C. thanks Dr. D. Golze and E. Makkonen for the help with CP2K and GPAW.

[1] T. Tsukuda and H. Häkkinen, *Protected Metal Clusters: From Fundamentals to Applications* (Elsevier, Amsterdam, 2015).

[2] E. Gwinn, D. Schultz, S. M. Copp, and S. Swasey, DNA-protected silver clusters for nanophotonics, Nanomaterials **5**, 180 (2015).

[3] Z. Yuan, Y.-C. Chen, H.-W. Li, and H.-T. Chang, Fluorescent silver nanoclusters stabilized by DNA scaffolds, Chem. Commun. **50**, 9800 (2014).

[4] R. R. Ramazanov, T. S. Sych, Z. V. Reveguk, D. A. Maksimov, A. A. Vdovichev, and A. I. Kononov, Ag-DNA emitter: Metal nanorod or supramolecular complex? J. Phys. Chem. Lett. **7**, 3560 (2016).

[5] J. T. Petty, M. Ganguly, I. J. Rankine, E. J. Baucum, M. J. Gillan, L. E. Eddy, J. C. Léon, and J. Müller, Repeated and folded DNA sequences and their modular Ag_{10}^{6+} cluster, J. Phys. Chem. C **122**, 4670 (2018).

[6] P. G. Lisinetskaya and R. Mitrić, Collective response in DNA-stabilized silver cluster assemblies from first-principles simulations, J. Phys. Chem. Lett. **10**, 7884 (2019).

[7] S. M. Copp, D. Schultz, S. Swasey, J. Pavlovich, M. Debord, A. Chiu, K. Olsson, and E. Gwinn, Magic numbers in DNA-stabilized fluorescent silver clusters lead to magic colors, J. Phys. Chem. Lett. **5**, 959 (2014).

[8] W. Guo, J. Yuan, Q. Dong, and E. Wang, Highly sequence-dependent formation of fluorescent silver nanoclusters in hybridized DNA duplexes for single nucleotide mutation identification, J. Am. Chem. Soc. **132**, 932 (2010).

[9] H.-C. Yeh, J. Sharma, I.-M. Shih, D. M. Vu, J. S. Martinez, and J. H. Werner, A fluorescence light-up Ag nanocluster probe that discriminates single-nucleotide variants by emission color, J. Am. Chem. Soc. **134**, 11550 (2012).

[10] G.-Y. Lan, C.-C. Huang, and H.-T. Chang, Silver nanoclusters as fluorescent probes for selective and sensitive detection of copper ions, Chem. Commun. **46**, 1257 (2010).

[11] S. W. Yang and T. Vosch, Rapid detection of microrna by a silver nanocluster DNA probe, Anal. Chem. **83**, 6935 (2011).

[12] T. Li, L. Zhang, J. Ai, S. Dong, and E. Wang, Ion-tuned DNA/Ag fluorescent nanoclusters as versatile logic device, ACS Nano **5**, 6334 (2011).

[13] J. Yu, S. Choi, C. I. Richards, Y. Antoku, and R. M. Dickson, Live cell surface labeling with fluorescent Ag nanocluster conjugates, Photochem. Photobiol. **84**, 1435 (2008).

[14] C. Cerretani, H. Kanazawa, T. Vosch, and J. Kondo, Crystal structure of a NIR-emitting DNA-stabilized Ag16 nanocluster, Angew. Chem. Int. Ed. **58**, 17153 (2019).

[15] D. J. E. Huard, A. Demissie, D. Kim, D. Lewis, R. M. Dickson, J. T. Petty, and R. L. Lieberman, Atomic structure of a fluorescent Ag8 cluster templated by a multistranded DNA scaffold, J. Am. Chem. Soc. **141**, 11465 (2019).

[16] X. Chen, E. Makkonen, D. Golze, and O. Lopez-Acevedo, Silver-stabilized guanine duplex: Structural and optical properties, J. Phys. Chem. Lett, **9**, 4789 (2018).

[17] L. A. Espinosa Leal, A. Karpenko, S. Swasey, E. G. Gwinn, V. Rojas-Cervellera, C. Rovira, and O. Lopez-Acevedo, The role of hydrogen bonds in the stabilization of silver-mediated cytosine tetramers, J. Phys. Chem. Lett. **6**, 4061 (2015).

[18] S. M. Swasey, N. Karimova, C. M. Aikens, D. E. Schultz, A. J. Simon, and E. G. Gwinn, Chiral electronic transitions in fluorescent silver clusters stabilized by DNA, ACS Nano **8**, 6883 (2014).

[19] S. M. Copp, P. Bogdanov, M. Debord, A. Singh, and E. Gwinn, Base motif recognition and design of DNA templates for fluorescent silver clusters by machine learning, Adv. Mater. **26**, 5839 (2014).

[20] S. M. Copp, A. Gorovits, S. M. Swasey, S. Gudibandi, P. Bogdanov, and E. G. Gwinn, Fluorescence color by data-driven design of genomic silver clusters, ACS Nano **12**, 8240 (2018).

[21] D. Schultz, K. Gardner, S. S. R. Oemrawsingh, N. Markešević, K. Olsson, M. Debord, D. Bouwmeester, and E. Gwinn, Evidence for rod-shaped DNA-stabilized silver nanocluster emitters, Adv. Mater. **25**, 2797 (2013).

[22] X. Chen, A. Karpenko, and O. Lopez-Acevedo, Silver-mediated double helix: Structural parameters for a robust DNA building block, ACS Omega **2**, 7343 (2017).

[23] X.-J. Lu and W. K. Olson, 3DNA: A software package for the analysis, rebuilding and visualization of three-dimensional nucleic acid structures, Nucl. Acids Res. **31**, 5108 (2003).

[24] J. Hutter, M. Iannuzzi, F. Schiffmann, and J. VandeVondele, CP2K: atomistic simulations of condensed matter systems, WIREs Comput. Mol. Sci. **4**, 15 (2014).

[25] J. W. Ponder and D. A. Case, Force fields for protein simulations, Adv. Protein Chem. **66**, 27 (2003).

[26] G. Lippert, J. Hutter, and M. Parrinello, A hybrid Gaussian and plane wave density functional scheme, Mol. Phys. **92**, 477 (1997).

[27] J. VandeVondele, M. Krack, F. Mohamed, M. Parrinello, T. Chassaing, and J. Hutter, QUICKSTEP: Fast and accurate density functional calculations using a mixed Gaussian and plane waves approach, Comput. Phys. Commun. **167**, 103 (2005).

[28] J. VandeVondele and J. Hutter, Gaussian basis sets for accurate calculations on molecular systems in gas and condensed phases, J. Chem. Phys. **127**, 114105 (2007).

[29] S. Goedecker, M. Teter, and J. Hutter, Separable dual-space Gaussian pseudopotentials, Phys. Rev. B **54**, 1703 (1996).

[30] C. Hartwigsen, S. Goedecker, and J. Hutter, Relativistic separable dual-space Gaussian pseudopotentials from H to Rn, Phys. Rev. B **58**, 3641 (1998).

[31] M. Krack, Pseudopotentials for H to Kr optimized for gradient-corrected exchange-correlation functionals, Theor. Chem. Acc. **114**, 145 (2005).

[32] J. P. Perdew, K. Burke, and M. Ernzerhof, Generalized Gradient Approximation Made Simple, Phys. Rev. Lett. **77**, 3865 (1996).

[33] S. Grimme, J. Antony, S. Ehrlich, and H. Krieg, A consistent and accurate *ab initio* parametrization of density functional dispersion correction (DFT-D) for the 94 elements H-Pu, J. Chem. Phys. **132**, 154104 (2010).

[34] T. Laino, F. Mohamed, A. Laio, and M. Parrinello, An efficient linear-scaling electrostatic coupling for treating periodic boundary conditions in QM/MM simulations, J. Chem. Theory Comput. **2**, 1370 (2006).

[35] T. Laino, F. Mohamed, A. Laio, and M. Parrinello, An efficient real space multigrid QM/MM electrostatic coupling, J. Chem. Theory Comput. **1**, 1176 (2005).

[36] J. Enkovaara, C. Rostgaard, J. J. Mortensen, J. Chen, M. Dulak, L. Ferrighi, J. Gavnholt, C. Glinsvad, V. Haikola, H. A. Hansen, H. H. Kristoffersen, M. Kuisma, A. H. Larsen, L. Lehtovaara, M. Ljungberg, O. Lopez-Acevedo, P. G. Moses, J. Ojanen, T. Olsen, V. Petzold, N. A. Romero, J. Stausholm-Møller, M. Strange, G. A. Tritsaris, M. Vanin, M. Walter, B. Hammer, H. Häkkinen, G. K. H. Madsen, R. M. Nieminen, J. K. Nørskov, M. Puska, T. T. Rantala, J. Schiøtz, K. S. Thygesen, and K. W. Jacobsen, Electronic structure

calculations with GPAW: a real-space implementation of the projector augmented-wave method, J. Phys.: Condens. Matter **22**, 253202 (2010).

[37] M. Walter, H. Häkkinen, L. Lehtovaara, M. Puska, J. Enkovaara, C. Rostgaard, and J. J. Mortensen, Time-dependent density-functional theory in the projector augmented-wave method, J. Chem. Phys. **128**, 244101 (2008).

[38] M. Kuisma, J. Ojanen, J. Enkovaara, and T. T. Rantala, Kohn-Sham potential with discontinuity for band gap materials, Phys. Rev. B **82**, 115106 (2010).

[39] R. van Leeuwen and E. J. Baerends, Exchange-correlation potential with correct asymptotic behavior, Phys. Rev. A **49**, 2421 (1994).

[40] V. Bonaĉić-Koutecky, V. Veyret, and R. Mitrić, *Ab initio* study of the absorption spectra of Ag_n ($n = 5$–8) clusters, J. Chem. Phys. **115**, 10450 (2001).

[41] O. Gritsenko, R. van Leeuwen, E. van Lenthe, and E. J. Baerends, Self-consistent approximation to the Kohn-Sham exchange potential, Phys. Rev. A **51**, 1944 (1995).

[42] M. Kuisma, A. Sakko, T. P. Rossi, A. H. Larsen, J. Enkovaara, L. Lehtovaara, and T. T. Rantala, Localized surface plasmon resonance in silver nanoparticles: Atomistic first-principles time-dependent density-functional theory calculations, Phys. Rev. B **91**, 115431 (2015).

[43] See Supplemental Material at http://link.aps.org/supplemental/10.1103/PhysRevMaterials.4.065601 for include more supplemental calculated ECD and optical absorption spectra, and calculated Barde charge of $Ag_6^{+2}@C_6$-$[Ag^+]_2$-C_6 at PBE0 level.

[44] M. Guidon, J. Hutter, and J. VandeVondele, Auxiliary density matrix methods for Hartree-Fock exchange calculations, J. Chem. Theory Comput. **6**, 2348 (2010).